nature nanotechnology

Article

https://doi.org/10.1038/s41565-023-01366-7

Proximal tubules eliminate endocytosed gold nanoparticles through an organelle-extrusion-mediated self-renewal mechanism

Received: 6 June 2022

Accepted: 3 March 2023

Published online: 17 April 2023

Check for updates

Yingyu Huang, Mengxiao Yu & Jie Zheng

Proximal tubules energetically internalize and metabolize solutes filtered through glomeruli but are constantly challenged by foreign substances during the lifespan. Thus, it is critical to understand how proximal tubules stay healthy. Here we report a previously unrecognized mechanism of mitotically quiescent proximal tubular epithelial cells for eliminating gold nanoparticles that were endocytosed and even partially transformed into large nanoassemblies inside lysosomes/endosomes. By squeezing ~5 µm balloon-like extrusions through dense microvilli, transporting intact gold-containing endocytic vesicles into the extrusions along with mitochondria or other organelles and pinching the extrusions off the membranes into the lumen, proximal tubular epithelial cells re-eliminated >95% of endocytosed gold nanoparticles from the kidneys into the urine within a month. While this organelle-extrusion mechanism represents a new nanoparticle-elimination route, it is not activated by the gold nanoparticles but is an intrinsic 'housekeeping' function of normal proximal tubular epithelial cells, used to remove unwanted cytoplasmic contents and self-renew intracellular organelles without cell division to maintain homoeostasis.

Driven by glomerular hydrostatic pressure[1] and regulated by the glomerular filtration membrane as a bandpass filter[2], renal clearance is often viewed as a passive process to rapidly eliminate engineered nanoparticles out of the body and reduce their systemic toxicity. However, the filtered nanoparticles can still actively interact with a variety of renal tubules (Fig. 1a), in which the proximal tubules (PTs) packed with dense mitochondria play a central role in the active uptake, reabsorption and metabolism of filtered substances[1]. With a dense brush boader composed of negatively charged microvilli and extending into the tubular cavities, proximal tubular epithelial cells (PTECs) can retain the filtered substances through contractile motions and effectively take them up[3]. Consequently, both endogenous low-molecular-weight proteins and exogenous substances including ultrasmall nanoparticles have been found inside PTECs[4,5]. For proteins, they could be reabsorbed back into the bloodstream as either intact entities through transcytosis[6] or amino acids after degradation inside the lysosomes[4]. Although inorganic nanoparticles such as polysiloxane nanoparticles and gold nanoparticles (AuNPs) are not biodegradable in the lysosomes, their accumulation in the PTECs and entire kidneys was still found to decrease with time[2,5]. Such a gradual removal of intracellular nanoparticles from the PTECs has been a long-standing mystery in the understanding of nanoparticle elimination in the kidneys[7].

Elimination of endocytosed nanoparticles at the cellular level is attributed to exocytosis mediated by different intracellular vesicles[8]. Lysosome-mediated exocytosis is the most common mechanism[9]. By fusing with the plasma membrane, the lysosomes release individual endocytosed nanoparticles back into the extracellular environment[9]. However, this process can be hindered once nanoparticles

Department of Chemistry and Biochemistry, The University of Texas at Dallas, Richardson, TX, USA. e-mail: mengxiao.yu@utdallas.edu; jiezheng@utdallas.edu

https://doi.org/10.1038/s41565-023-01366-7

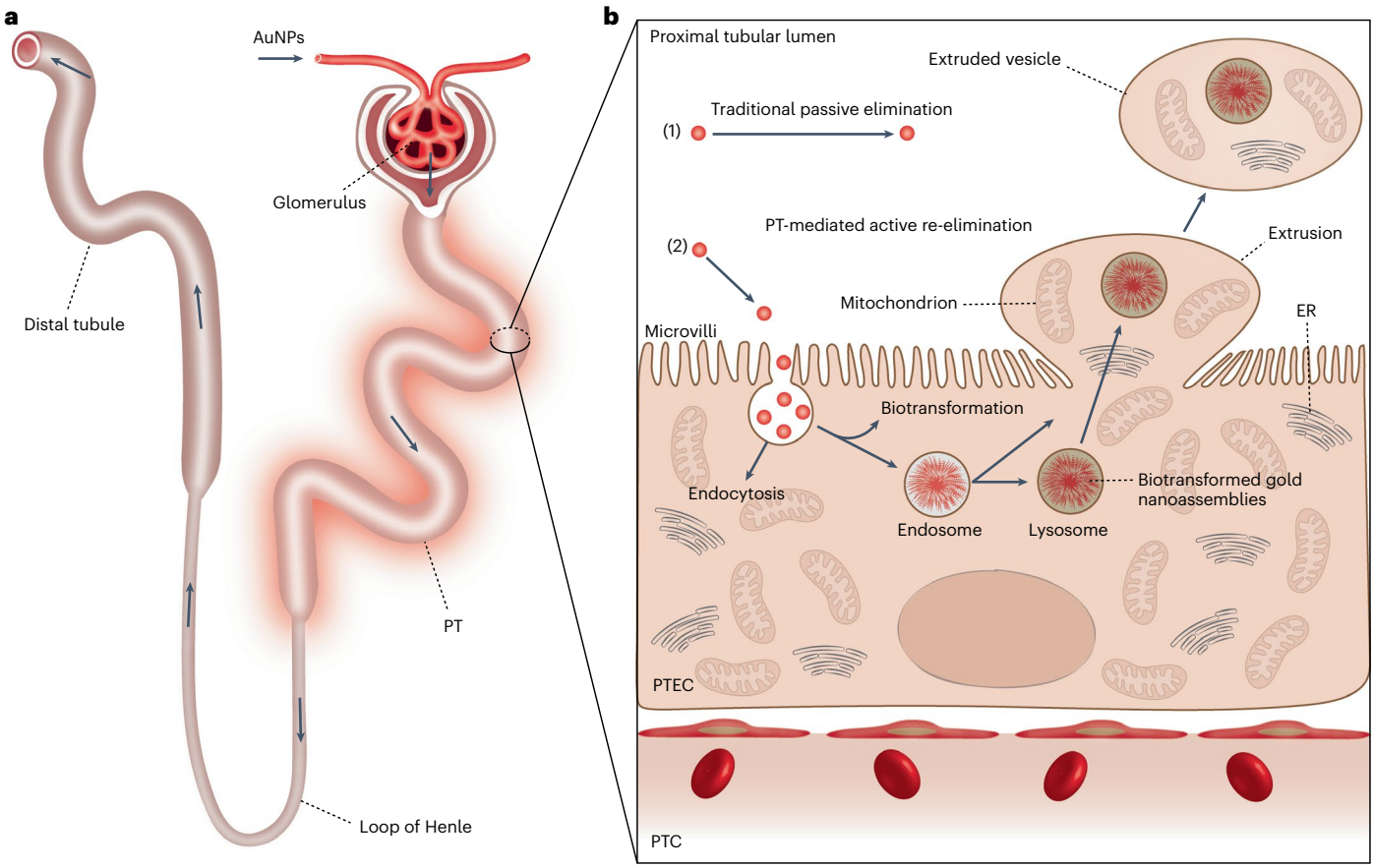

Fig. 1 | Elimination process and interaction of renal-clearable engineered nanoparticles in the kidneys. a, Renal-clearable engineered nanoparticles (for example, AuNPs) will be first filtered through the glomerulus. The filtered nanoparticles will then enter the PTs, followed by travel through the loop of Henle, the distal tubules and the collecting ducts, and eventually entering the bladder through the ureters. Among all the components of the nephron, the PT is the most active site of uptake of the filtered nanoparticles due to the densely packed microvilli on its luminal surface. **b**, In addition to the traditional passive elimination of nanoparticles through the kidneys, with little involvement of cellular internalization and metabolism (1), we discovered a PT-mediated active re-elimination pathway of AuNPs involving endocytosis, biotransformation in the endosomes/lysosomes and cellular elimination through organelle extrusion on the luminal membrane of PTs (2). The 2–3 nm AuNPs can be internalized by PTECs through endocytosis. The endocytosed AuNPs are then partially biotransformed into 200–300 nm, large nanoassemblies inside endosomes/lysosomes. By squeezing ~5 μm balloon-like extrusions through dense microvilli, transporting intact gold-containing endosomes or lysosomes into the extrusions along with mitochondria or other organelles and pinching off the extrusions from the cell membrane into the lumen, PTECs re-eliminated endocytosed AuNPs, including those large biotransformed nanoassemblies, into the urine, and they were further cleared out of the body afterward. PTC, peritubular capillary.

are biochemically transformed into large nanoassemblies inside the lysosomes[10,11]. Additionally, nanoparticles in early endosomes could also be translocated into multivesicular bodies first, followed by being released into the extracellular space through membrane fusion between the multivesicular bodies and plasma membrane[12,13]. The released nanoparticles are encapsulated in either exosomes (~100 nm) or extracellular microvesicles (~1–2 μm). Moreover, some nanoparticles could also take advantage of secretion machineries in the gland cells to enter the extracellular spaces[14]. However, the detailed mechanism for eliminating endocytosed nanoparticles in the PTs down to the subcellular level is still largely unknown.

Using renal-clearable AuNPs as multimodality probes that can be filtered through the kidneys and readily detected with inductively coupled plasma mass spectrometry (ICP-MS) and optical and electron microscopies, we discovered an unrecognized mechanism of PTECs for eliminating endocytosed 2–3 nm AuNPs and their 200–300 nm nanoassemblies back into the urine (Fig. 1b). We found that PTECs were able to directly eject entire gold-containing lysosomes/endosomes along with other organelles (mitochondria, lysosomes without gold, smooth endoplasmic reticulum, apical vacuoles or even an entire nucleus in some rare cases) into the proximal tubular lumen to form ~5 μm extruded vesicles. This organelle-extrusion-mediated elimination of AuNPs represents a nanoparticle-elimination mechanism distinct from those membrane-fusion-mediated ones. However, this extrusion process is not activated by the AuNPs but by an intrinsic physiological 'housekeeping' function of normal PTs, used to remove unwanted substances and renew intracellular organelles without cell division, which, however, was significantly reduced once the tubules were injured.

Endocytosis and re-elimination of AuNPs by PTs

While the glomerulus is known to dictate the filterability of engineered nanoparticles in the kidneys[2,15], we find that nanoparticle clearance out of the kidneys is also regulated by the PTs through PTEC-mediated endocytosis and active re-elimination. Since the dense negatively charged microvilli on the luminal surface of PTECs is known to enhance the uptake of positively charged endogenous proteins[16], we synthesized two types of renal-clearable PEGylated AuNPs (PEG, poly(ethylene glycol)) with the same core sizes (~2.6 nm) but opposite zeta potentials (positively charged and negatively charged AuNPs, that is, (+)-AuNPs

https://doi.org/10.1038/s41565-023-01366-7

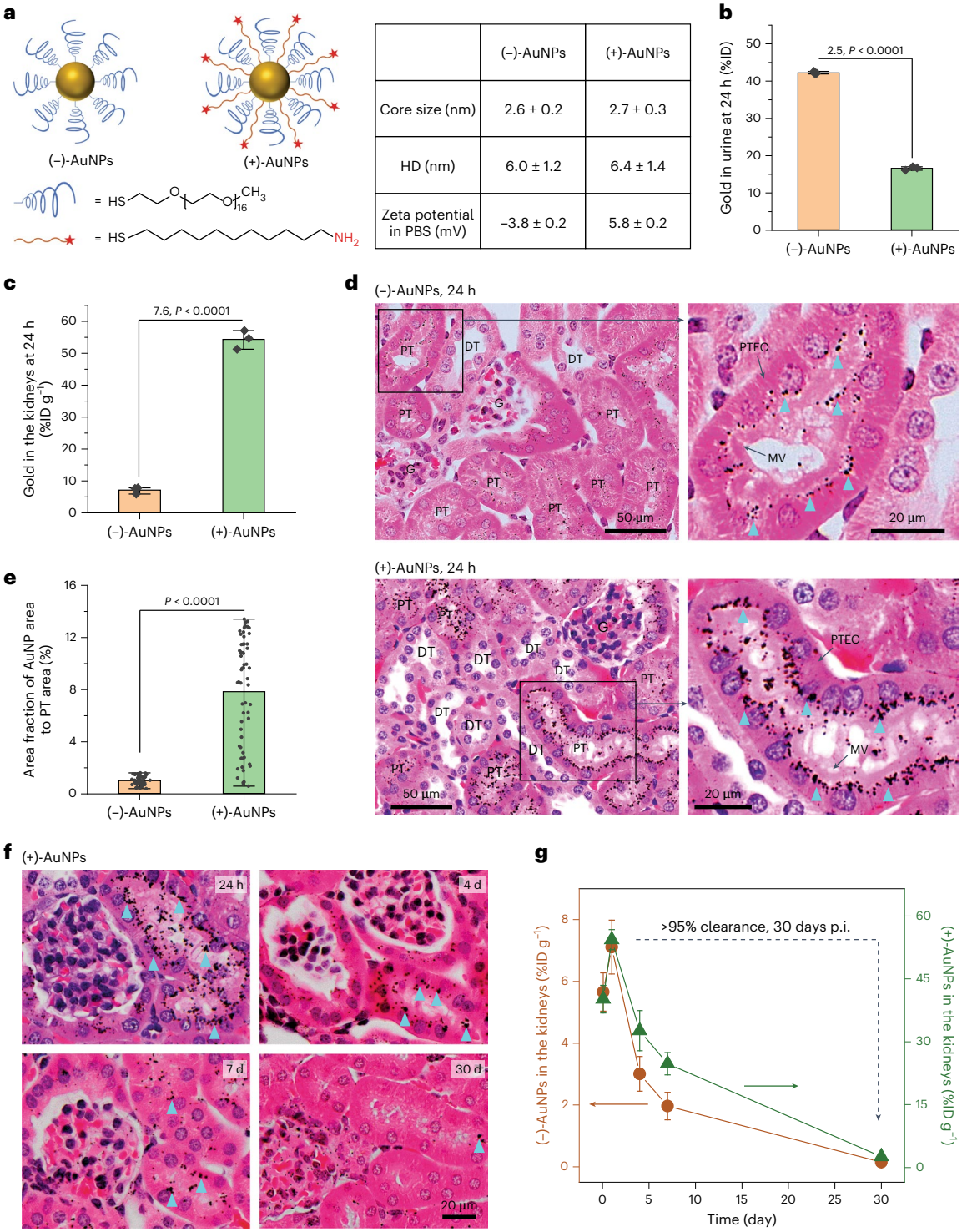

	(–)-AuNPs	(+)-AuNPs
Core size (nm)	2.6 ± 0.2	2.7 ± 0.3
HD (nm)	6.0 ± 1.2	6.4 ± 1.4
Zeta potential in PBS (mV)	–3.8 ± 0.2	5.8 ± 0.2

Fig. 2 | Endocytosis and re-elimination of the PEGylated AuNPs by PTECs in vivo. a, Design and characterizations of (−)-AuNPs and (+)-AuNPs via coating AuNPs with PEG methyl ether thiol (Molecular weight, 800 Da) or PEG methyl ether thiol together with amine-terminated positively charged 11-amino-1-undecanethiol. HD, hydrodynamic diameters. **b**, Quantification of the amount of gold in the urine collected at 24 h p.i. of the AuNPs, which was measured by ICP-MS. $P = 4.54 \times 10^{-7}$. $N = 3$ mice for each group. **c**, Quantification of the amount of gold in the kidneys harvested at 24 h p.i. of the AuNPs, measured with ICP-MS. $P = 3.86 \times 10^{-4}$. $N = 3$ mice for each group. **d**, Representative images of silver-enhanced and hematoxylin and eosin (H&E)-stained tissue sections of the kidneys obtained at 24 h p.i. of (−)-AuNPs (upper) and (+)-AuNPs (lower). Silver-enhanced AuNPs are indicated by blue triangles. The righthand images show zoomed-in views of the areas in the boxes. G, glomerulus; DT, distal tubules; MV, microvilli. **e**, Quantification of the area fraction of silver-enhanced AuNPs in the entire cross-section of a PT. $P = 3.50 \times 10^{-18}$. $N = 60$ and 59 PT cross-sections for (−)-AuNPs and (+)-AuNPs, respectively. **f**, Representative images of silver-enhanced and H&E-stained kidney tissue sections at 24 h, 4 days, 7 days and 30 days p.i. of (+)-AuNPs. Silver-enhanced AuNPs are indicated by blue triangles. **g**, The amount of gold in the kidneys was measured with ICP-MS at different time points (2 h, 24 h, 4 days, 7 days and 30 days) after injection of (+)-AuNPs (green line) and (−)-AuNPs (orange line). Over 95% (that is, ((Amount at 24 h − Amount at 30 days)/Amount at 24 h) × 100%) of accumulated AuNPs were eliminated out of the kidneys within one month. $N = 3$ mice for each time point. Data are presented as mean ± s.d. (standard deviation) in **b**, **c**, **e** and **g**. Two-sided Student's *t*-test was performed at the 0.05 significance level in **b**, **c** and **e**. Representative images are presented out of images acquired from three independent samples in **d** and **f**.

https://doi.org/10.1038/s41565-023-01366-7

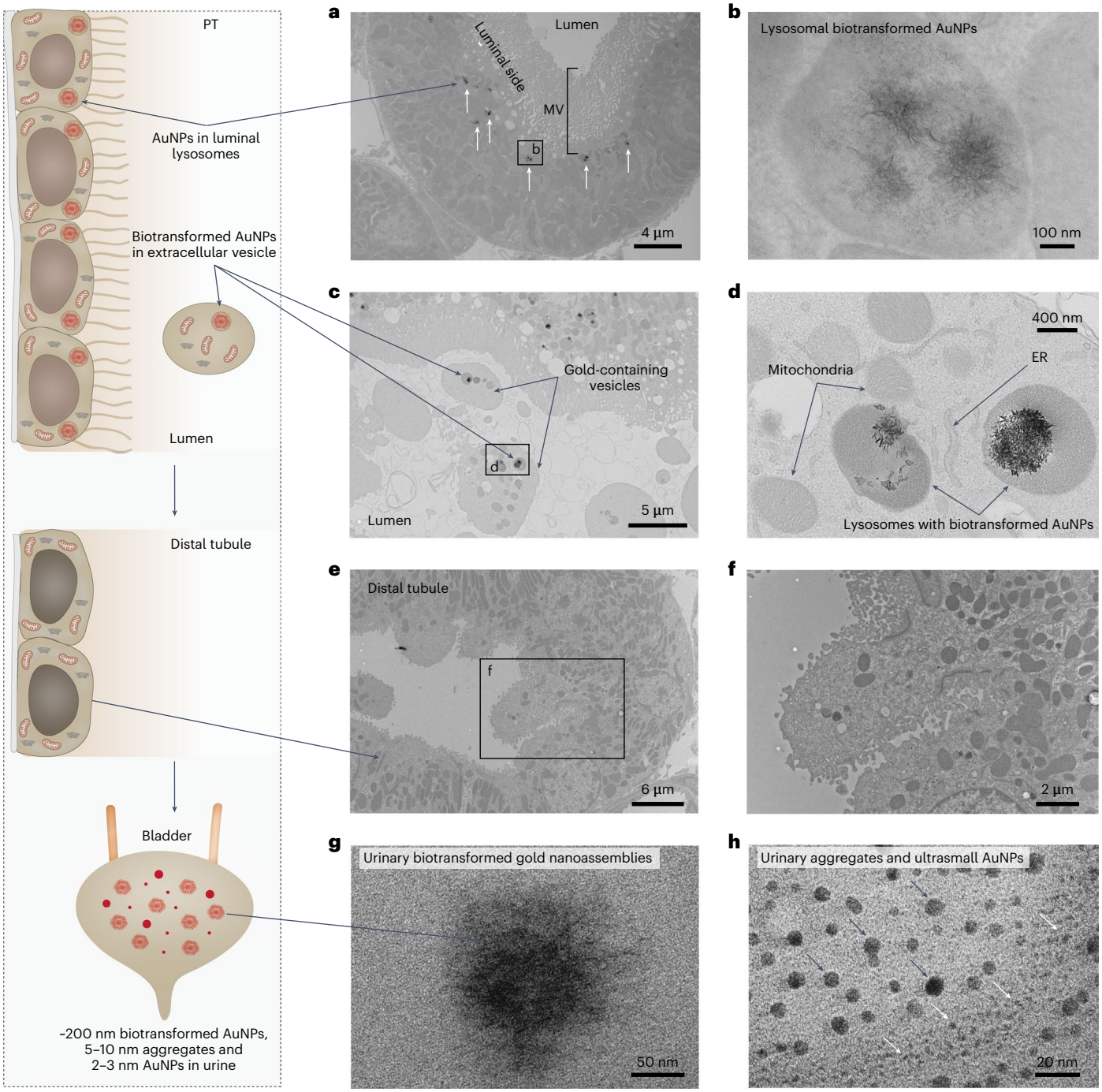

Fig. 3 | Biotransformation and re-excretion of endocytosed (+)-AuNPs by PTs. a, A representative EM image of PTs at 24 h p.i. of (+)-AuNPs showing the intracellular (+)-AuNPs located in lysosomes of PTECs on the luminal side (labelled by arrows). The labelled box is the area shown in **b**. **b**, A representative EM image of the biotransformed 200–300 nm flower-like gold nanoassemblies composed of nanofibres in a lysosome of PTEC. **c**, A representative EM image of extracellular vesicles in a proximal tubular lumen that contain lysosome-encapsulated biotransformed AuNPs and other organelles. **d**, A magnified image of the extracellular vesicle in **c** containing lysosome-encapsulated biotransformed AuNPs, mitochondria and smooth ER. **e**,**f**, Representative EM images of distal tubules showing that no biotransformed AuNPs were found inside the distal tubules at 24 h p.i. **g**,**h**, Representative EM images of biotransformed gold nanostructures, including ~200 nm gold nanoassemblies (**g**) and 5–10 nm AuNPs (**h**, indicated by black arrows), found in the urine within 24 h p.i. of (+)-AuNPs, in addition to ultrasmall AuNPs with an original size of 2–3 nm in the urine (**h**, indicated by white arrows). No gold or silver enhancement staining was used for EM samples. Representative EM images in **a**, **c**, **e**, **g** and **h** are presented out of images acquired from three independent samples. The image along the left side shows a schematic of the process.

and (−)-AuNPs; Fig. 2a and Supplementary Figs. 1 and 2) to unravel the charge dependency in the PT uptake of nanoparticles. Although the hydrodynamic diameters (HDs) of both AuNPs are ~6.0 nm (Supplementary Fig. 1) and below the glomerular filtration threshold (~6–8 nm), the 24 h renal clearance efficiency of (+)-AuNPs is 16.62 ± 0.38 %ID (%ID, percentage of injection dose) post intravenous injection (p.i.), ~2.5 times lower than that of (−)-AuNPs (42.21 ± 0.29 %ID; Fig. 2b) due to their different interactions with the organs. The blood concentrations

https://doi.org/10.1038/s41565-023-01366-7

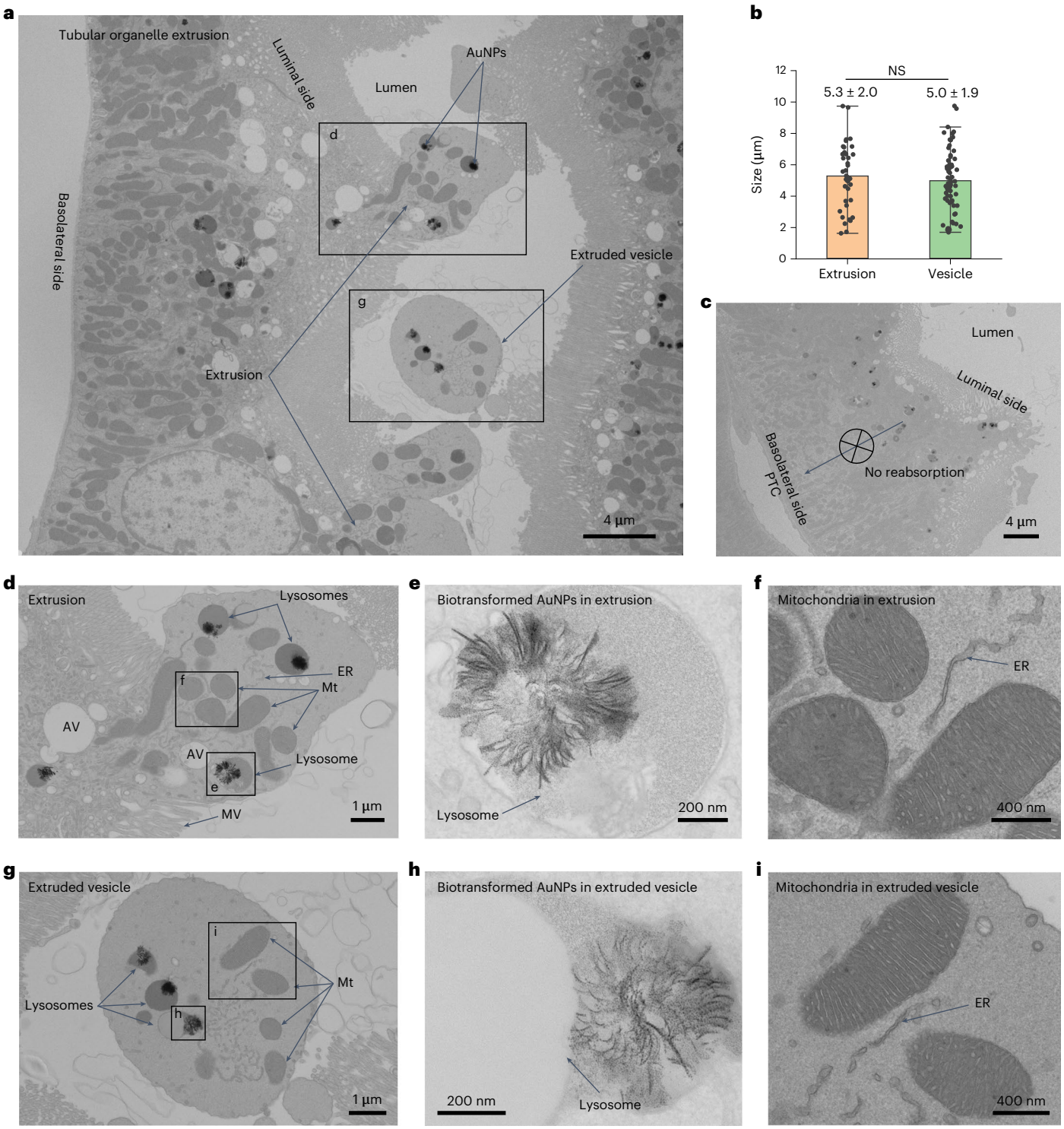

Fig. 4 | Nanoparticle elimination by PTECs through an organelle-extrusion mechanism. a, A representative EM image of PTs at 24 h p.i. of (+)-AuNPs showing the tubular organelle-extrusion process: a balloon-like fraction of cytoplasm was squeezed through the microvilli and extruded into the extracellular lumen space (labelled as extrusions) to form the extracellular vesicles in the lumen (labelled as extruded vesicles). AuNPs are labelled with arrows. The labelled boxes indicate areas shown in a zoomed-in view in other panels. **b**, No significant difference (NS) is seen in the sizes of extrusions on the luminal membrane ($N = 38$, mean ± s.d.) and extruded vesicles in the tubular lumen ($N = 67$, mean ± s.d.). $P = 0.47$. Two-sided Student's t-test was performed at the 0.05 significance level. **c**, A representative EM image of PTs showing no sign of extrusion on the basolateral side of the PTs and no sign of endocytosed AuNPs on the luminal side migrating to the basolateral side of the PTs and being reabsorbed into the peritubular capillary. **d**, Magnified EM image of an extrusion in **a**. The extrusion is devoid of microvilli but contains intracellular organelles including mitochondria (Mt), lysosomes (with or without AuNPs), apical vacuoles (AV) and smooth ER. **e**, Magnified EM image of a lysosome encapsulating biotransformed AuNPs in the extrusion in **d**. **f**, Magnified EM image of mitochondria and ER in the membrane extrusion in **d**. **g**, Magnified EM image of an extruded vesicle in a proximal tubular lumen in **a**. Like the extrusion on the luminal membrane, the extruded vesicle also contained similar organelles such as mitochondria, lysosomes and smooth ER. **h**, Magnified EM image of lysosome-encapsulated biotransformed AuNPs in the extruded vesicle in **g**. **i**, Magnified EM image of mitochondria and ER in the extruded vesicle in **g**. No gold or silver enhancement staining was used for EM samples. Representative EM images in **c**, **d** and **g** are presented out of images acquired from three independent samples.

https://doi.org/10.1038/s41565-023-01366-7

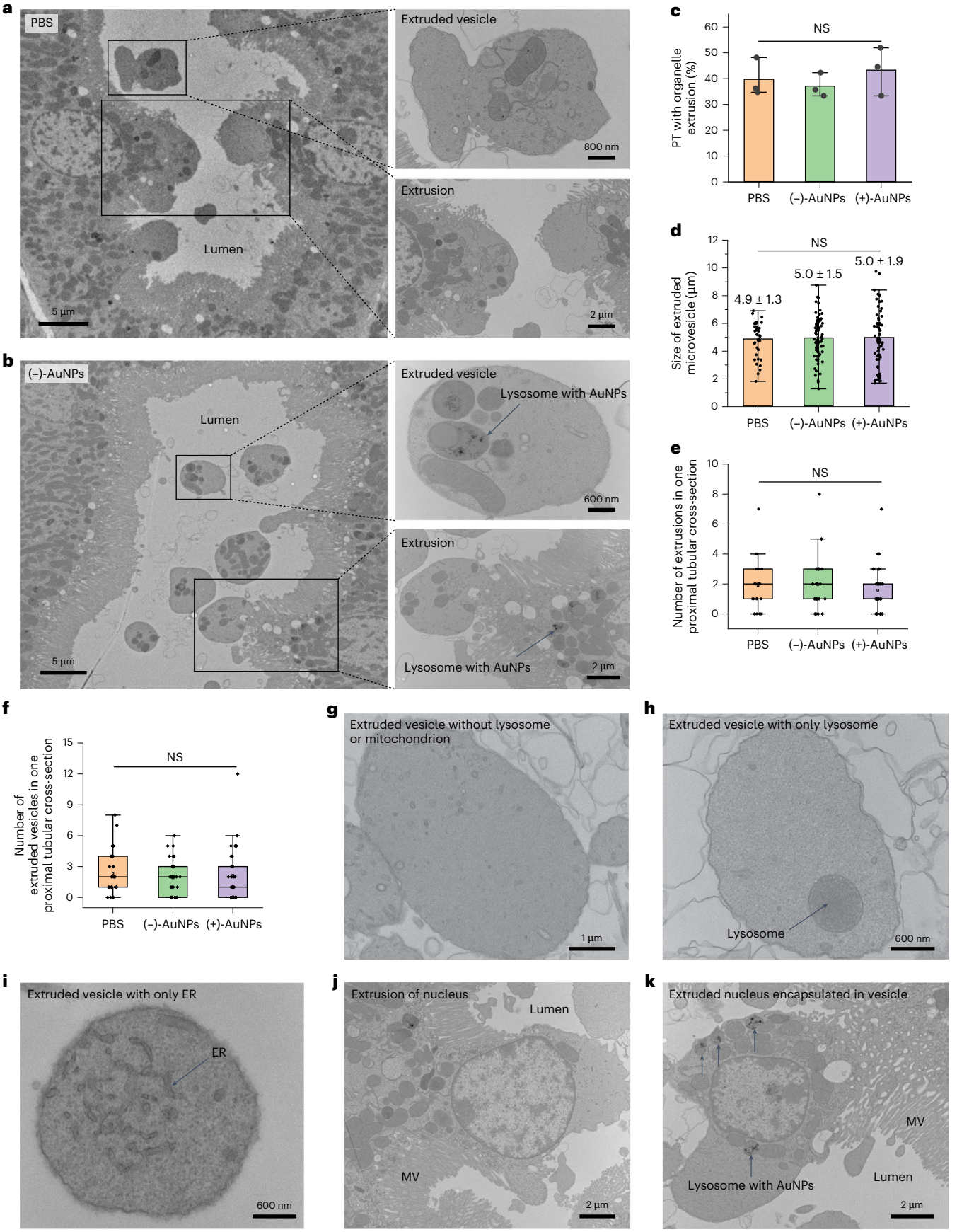

of both AuNPs were very low at 24 h p.i. (2.99 ± 0.02 %ID g^{-1} for (–)-AuNPs and 1.61 ± 0.44 %ID g^{-1} for (+)-AuNPs; %ID g^{-1}, %ID per gram of blood or tissue; Supplementary Fig. 3); however, the kidney accumulation of (+)-AuNPs reached 54.35 ± 2.39 %ID g^{-1} at 24 h p.i., about eight times higher than that of (–)-AuNPs (7.11 ± 0.87 %ID g^{-1}; Fig. 2c), even though a much larger portion of (+)-AuNPs (33.22 ± 2.38 %ID g^{-1}) was also taken

Fig. 5 | Organelle extrusion is a native physiological function of PTs. **a**,**b**, Representative EM images of tubular organelle extrusions in PBS-injected mice (**a**) and (−)-AuNP-injected mice (**b**) at different magnifications. **c**–**f**, Quantitative analyses on the percentage of PTs with extrusions (**c**), sizes of extruded vesicles in the tubular lumen (**d**), number of extrusions of the proximal tubular cross-section (**e**) and number of extruded vesicles of the proximal tubular cross-section (**f**) derived from EM imaging studies of the PTs among mice treated with PBS, (−)-AuNPs and (+)-AuNPs. In **c**, $N = 3$ tissue sections of three individual tissue blocks for each group, and more than 70 proximal tubular cross-sections were analysed for each tissue block. $P = 0.61$. In **d**, for PBS, (−)-AuNP and (+)-AuNP injection, respectively, $N = 38$, 74 and 67 extruded vesicles found in three tissue sections from three individual tissue blocks. $P = 0.95$. In **e** and **f**, $N = 29$ proximal tubular cross-sections analysed in each group. $P = 0.64$ in **e**. $P = 0.74$ in **f**. Data are presented as mean ± s.d. in **c** and **d**. Data are analysed using one-way analysis of variance at the 0.05 significance level in **c**–**f**. The boxes in **e** and **f** range from the 25th percentile (the first quartile, top of the boxes) to the 75th percentile (the third quartile, bottom of the boxes). The lines in the boxes present the median values. The whiskers are the lowest and highest points within 1.5 times the interquartile range of the lower and higher quartiles. **g**, A representative EM image of an extruded vesicle containing neither lysosomes nor mitochondria. **h**, A representative EM image of an extruded vesicle containing only lysosome. **i**, A representative EM image of an extruded vesicle containing only ER. **j**, A representative EM image of an extrusion containing a nucleus in PBS-injected mice. **k**, A representative EM image of an extruded vesicle containing a nucleus and lysosome-encapsulated AuNPs and their nanoassemblies (indicated by arrows) in (−)-AuNP-injected mice. Representative EM images in **g**–**k** are presented out of images acquired from three independent samples.

up by the liver than the portion of (−)-AuNPs (3.91 ± 0.55 %ID g^{-1}) due to the known charge selectivity in the liver uptake[17,18] (Supplementary Fig. 3). The histological studies further show that the kidney accumulation of the AuNPs 24 h p.i. is mainly because of uptake by the PTs. As shown in Fig. 2d,e, the PT is a major site for uptake of both AuNPs at 24 h p.i., whereas very few AuNPs were found in the other components of the nephron (Supplementary Figs. 4–7). Such selectivity to the PTs is very likely because densely packed microvilli on the apical membrane of the PTs are known to increase the surface area of the PTECs and facilitate the adsorption of filtered substances[3]. Consistent with the higher kidney accumulation of (+)-AuNPs than (−)-AuNPs, more (+)-AuNPs were internalized by PTECs than (−)-AuNPs (Fig. 2d,e and Supplementary Fig. 8). Clathrin-mediated endocytosis was further identified to be involved in the uptake of (+)-AuNPs by PTs, through chlorpromazine inhibition studies (Supplementary Fig. 9). These results confirmed the charge dependency involved in the nanoparticle endocytosis by PTs. Despite the high uptake of (+)-AuNPs by the PTs, the endocytosed (+)-AuNPs were still effectively eliminated out of the PTs without inducing pathological damages within one month (Fig. 2f and Supplementary Fig. 10). Consistently, the kidney accumulation of (+)-AuNPs decreased from 54.35 ± 2.39 %ID g^{-1} at one day p.i. to 2.62 ± 0.27 %ID g^{-1} at 30 days p.i. (Fig. 2g and Supplementary Fig. 11). As a result, 95.2% of the endocytosed AuNPs in the kidneys at one day p.i. were re-eliminated after one month (Fig. 2g). A similar trend was also observed from (−)-AuNPs (Fig. 2g and Supplementary Fig. 11). All these findings show that the PTs can endocytose the filtered nanoparticles efficiently through charge-mediated interactions and can also re-eliminate the endocytosed AuNPs effectively within a month.

Biotransformation and excretion of AuNPs by PTs

Biotransformation, an intrinsic cellular metabolism of endocytosed substances, has been found to hinder nanoparticle exocytosis[10,11]. To unravel the fate of endocytosed AuNPs at a subcell level, we used electron microscopy (EM) to image the PTs down to nanometre resolution. Ultrastructure imaging studies show that all the (+)-AuNPs inside the PTECs were stored in either lysosomes (~93%) or endosomes (~7%) near the luminal cell membrane 24 h p.i., further confirming that the AuNPs were internalized by PTECs through endocytosis (Fig. 3a and Supplementary Fig. 12). In addition to monodispersed 2–3 nm AuNPs, a large portion of the nanoparticles were biochemically transformed into large gold nanoassemblies of 216 ± 55 nm with diverse morphologies within 24 h p.i., including flower-like assemblies of gold nanofibres with lengths of ~20 to 50 nm (Fig. 3b) and aggregates of larger AuNPs of 5–10 nm, as well as hybrid assemblies of nanofibres and 5–10 nm AuNPs (Supplementary Figs. 13 and 14). Similar morphologies of nanoassemblies were observed in both lysosomes and endosomes (Supplementary Fig. 15). This was not limited to (+)-AuNPs; (−)-AuNPs were also biotransformed after endocytosis (Supplementary Fig. 16). We further imaged (+)-AuNPs in the liver and found that the (+)-AuNPs were endocytosed by Kupffer cells and were also biotransformed into the flower-like nanoassemblies in the lysosomes (Supplementary Fig. 17). Similar biotransformation was also observed from 2–3 nm dye-conjugated AuNPs inside cancer cells[19] and 4 nm AuNPs inside fibroblast cells[10]. In addition to the Balb/c mouse model, a metallothionine (MT) knockout mouse model was also used to investigate the biotransformation mechanism. The observation of a similar biotransformation of (+)-AuNPs in PTECs suggests that MT is not essential to the AuNP biotransformation (Supplementary Fig. 18). On the other hand, we observed a size increase of (+)-AuNPs from 2.5 nm to 10 nm as well as self-assembly of the 10 nm AuNPs into a unique ~150 nm dendritic gold nanostructure after incubation with H_2O_2, while the size of (+)-AuNPs remained almost unchanged after incubation with glutathione and MT at pH 4.5 in the test tubes (Supplementary Fig. 19), implying that reactive oxygen species might play a more important role in the intracellular biotransformation of

Fig. 6 | Nanoparticle endocytosis and organelle extrusion significantly reduced in PTs with cisplatin-induced injury. **a**–**c**, Representative pathological and EM images of the PTs in cisplatin-injected mice showing three distinct injury statuses. **a**, A normal-appearing PT with no obvious structural damage in the pathology and no ultrastructural damage in the EM image. A high uptake of (+)-AuNPs was observed (AuNPs are indicated by white arrows). **b**, A mildly damaged PT. Intracellular vacuolization is clearly identified in the pathology. Both vacuolization and mitochondrial fragmentation are observed in the EM image. Less uptake of (+)-AuNPs was observed (AuNPs are indicated by white arrows). **c**, A severely damaged PT. Degenerated proximal tubular structure is observed. Consistently, cell apoptosis with apoptotic bodies is observed in the EM image. Almost no (+)-AuNPs are observed in the severely damaged PTs. **d**, Quantification of the area fraction of silver-enhanced AuNPs in the entire cross-section of a PT in normal-appearing, mildly damaged and severely damaged PTs. $N = 30$, 30 and 32 proximal tubular cross-sections in H&E-stained kidney tissue slides were analysed for normal, mildly damaged and severely damaged PTs, respectively. Data are presented as mean ± s.d. $P = 5.16 \times 10^{-18}$ between normal and mild. $P = 3.75 \times 10^{-5}$ between mild and severe. Two-sided Student's *t*-test was performed at the 0.05 significance level. **e**, Representative EM images of the extrusion and biotransformation of lysosomal AuNPs in PTs with a mild injury. The biotransformation of AuNPs was unaffected in mildly damaged PTs. **f**, Percentages of PTs with organelle extrusion in normal mice and cisplatin-treated mice after (+)-AuNP injection showing that tubular organelle extrusion was significantly reduced in acute tubular injury. $N = 3$ tissue sections from three individual tissue blocks, mean ± s.d. More than 70 proximal tubular cross-sections were analysed for each tissue block. Two-sided Student's *t*-test was performed at the 0.05 significance level. **g**,**h**, Representative EM images of an autophagosome and apoptotic body in cisplatin-induced severely damaged PTs. No gold or silver enhancement staining was used for EM samples.

https://doi.org/10.1038/s41565-023-01366-7

AuNPs than thiolated peptides and proteins, through their destabilization; however, the detailed biotransformation mechanism still needs further investigation.

While such large gold nanoassemblies were expected to be permanently stored in the cytoplasm according to previous understanding of nanoparticle exocytosis[10,11], we observed them in extracellular vesicles of ~5 μm in the proximal tubular lumen (Fig. 3c,d and Supplementary Fig. 20). Unlike the observation of individual nanoparticles released to the extracellular space in lysosome-mediated exocytosis[9], the (+)-AuNPs and large gold nanoassemblies remained encapsulated

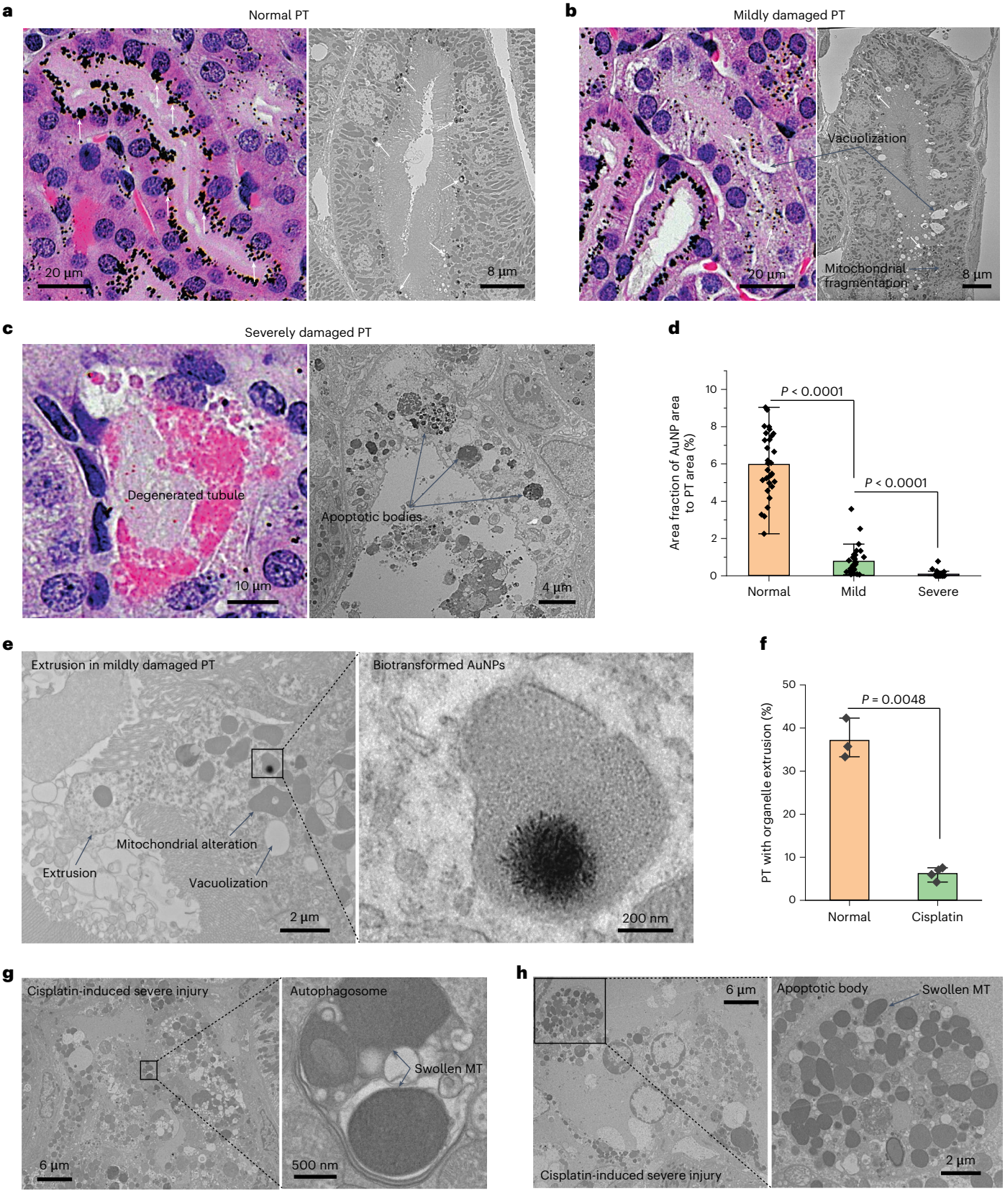

inside the intact lysosomes (~92%) or endosomes (~8%) in those ~5 μm extracellular vesicles (Supplementary Fig. 20). More astonishingly, along with those lysosomes/endosomes containing AuNPs and gold nanoassemblies, we also observed other organelles such as mitochondria and smooth endoplasmic reticulum (ER) in these large extracellular vesicles (Fig. 3d and Supplementary Fig. 20). Very few endocytosed AuNPs or gold nanoassemblies were observed in distal tubules (Fig. 3e,f and Supplementary Fig. 21) and collecting ducts (Supplementary Fig. 22), implying that the downstream nephron components were less involved in the uptake of AuNPs and the re-uptake of the extracellular vesicles. However, in the urine collected within 24 h p.i., we found the biotransformed gold nanostructures (including ~200 nm flower-like assemblies of gold nanofibres and 5–10 nm gold aggregates) along with ultrasmall AuNPs with their original size of 2–3 nm (Fig. 3g,h and Supplementary Fig. 23), indicating that the AuNPs re-excreted by PTECs were eventually cleared into the urine, consistent with the observation of the gradual elimination of the AuNPs out of the PTs and kidneys (Fig. 2f,g).

Organelle-extrusion-mediated elimination by PTs

Membrane fusion is an essential step in currently known nanoparticle exocytosis mediated by intracellular vesicles[8,9,12]. However, the observation of an intact lysosome encapsulating AuNPs and gold nanoassemblies in ~5 μm extracellular vesicles accompanied by other organelles implies an undiscovered nanoparticle-elimination pathway in the kidneys. Thus, we further examined the events on the plasma membrane of PTECs with EM and observed that a balloon-like fraction of cytoplasm with an average diameter of ~5 μm was exclusively squeezed through the dense microvilli and extruded into the extracellular lumen space rather than on basolateral side (Fig. 4a–c and Supplementary Figs. 24 and 25). Along with the extrusion of the cytoplasm on the luminal membrane, lysosome-encapsulated AuNPs and gold nanoassemblies, mitochondria and smooth ER were transported into the extrusions (Fig. 4d–f and Supplementary Fig. 24). Compared to the extracellular vesicles in the tubular lumen (Fig. 4g and Supplementary Fig. 20), the observed extrusions shared the same features in size (Fig. 4b) and contents including biotransformed AuNPs encapsulated in lysosomes, lysosomes without gold, mitochondria, smooth ER and apical vacuoles (Fig. 4d–i and Supplementary Fig. 24), suggesting that the extracellular vesicles originated from the extrusions on the plasma membrane, followed by a pinching off of the membranes and release to the tubular cavities. We did not observe the migration of AuNPs on the luminal side to the basolateral side of the PTs (Fig. 4c and Supplementary Fig. 25), indicating that endocytosed AuNPs were not reabsorbed back into the bloodstream from the basolateral side. Given the ability of EM imaging in differentiating the segment far from the glomerulus (S_3) from those close ones (S_1 and S_2) in PTs[20], we found that the cellular uptake of AuNPs and the organelle-extrusion process also occurred in the S_3 segment (Supplementary Fig. 26), indicating that the cellular uptake and the extrusion process are not specific to those segments close to the glomerulus (Supplementary Fig. 4). Moreover, we further examined the organelle-extrusion process in vitro in human kidney proximal tubular cells (HK-2) and observed a similar extrusion of cytoplasm on the cell membrane and extracellular vesicles adjacent to cells, with the extrusion containing mitochondria and lysosomes with or without AuNPs (Supplementary Fig. 27), implying that organelle extrusion is an intrinsic biological process of proximal tubular cells.

Organelle extrusion as a normal physiological function

The observation of the extrusion and elimination of endocytosed AuNPs along with different organelles inevitably leads to a fundamental question of whether this process was activated by the AuNPs or not. Our further studies show that organelle extrusion in the PTs also occurred in mice treated with phosphate-buffered saline (PBS; Fig. 5a and Supplementary Fig. 28) and (−)-AuNPs (Fig. 5b and Supplementary Fig. 29). Among the PBS, (−)-AuNP and (+)-AuNP groups, there were no significant differences in the percentages of PTs with tubular extrusion (Fig. 5c), the sizes of the extruded vesicles (Fig. 5d) or the numbers of extrusions (Fig. 5e), or the numbers of extruded vesicles (Fig. 5f) in the PTs. While mitochondria were observed in the tubular extruded vesicles, we also found that about 40% of vesicles contained no mitochondria (Supplementary Fig. 30). Some extruded vesicles contained neither mitochondria nor lysosomes (Fig. 5g and Supplementary Fig. 31), some contained only lysosomes (Fig. 5h and Supplementary Fig. 31) and some contained only ER (Fig. 5i). In some rare cases (~2%), we even observed an entire nucleus extruded out, together with AuNP-containing lysosomes (Fig. 5k and Supplementary Fig. 32). These results suggest that the types of organelles extruded out of the cell are also independent of the AuNP uptake. Although these organelles were eliminated out of the cytoplasm, pathological studies confirm that the PTECs remained healthy, and no elevation of renal function biomarkers was observed (Supplementary Fig. 33). Combining all these results, we conclude that the observed organelle extrusion is not activated by the AuNPs but is an intrinsic physiological function of normal PTs to self-renew their endogenous organelles and cytoplasmic contents.

Endocytosis and organelle extrusion in injured PTs

While organelle extrusion is a normal function of PTs, we also unravelled how drug-induced proximal tubular injury impacts organelle extrusion of nanoparticles. Using a well-known nephrotoxic chemodrug, cisplatin[21], we established a mouse model with acute but heterogeneous focal proximal tubular injuries (Supplementary Fig. 34) and identified three types of PTs with distinct pathological features using EM on the same tissue section: (1) PTs appearing normal, without detectable pathological damages, by optical microscopy and EM (Fig. 6a and Supplementary Fig. 35), (2) mildly damaged PTs with cell vacuolization and mitochondrial fragmentation (Fig. 6b and Supplementary Fig. 36) and (3) and severely damaged and degenerated PTs with cell apoptosis (Fig. 6c and Supplementary Fig. 37). We found that the endocytosis of (+)-AuNPs by the PTs declined as the injury progressed. While the tubules appearing normal still internalized the AuNPs, mildly injured tubules had a significantly reduced AuNP uptake, and very few AuNPs were observed inside the severely injured tubules (Fig. 6a–d and Supplementary Fig. 38). Although the uptake efficiencies dramatically decreased as tubular injury occurred, the biotransformation of endocytosed AuNPs remained the same in the injured cells as in normal cells (Fig. 6e and Supplementary Figs. 35 and 36). However, the organelle extrusion also significantly decreased in injured PTs. For (+)-AuNP-injected mice, the percentage of PTs with organelle extrusions or extruded vesicles decreased from 37.1 ± 4.6% in the normal mice to 6.2 ± 1.5% in the cisplatin model (Fig. 6f). In addition, the observed organelle extrusions in the cisplatin model mainly originated from tubules appearing normal or with mild injury (Fig. 6e and Supplementary Fig. 36). No organelle extrusion was observed in the severely damaged tubules. Moreover, once the PTs were severely injured by cisplatin, we frequently observed autophagosomes and apoptotic bodies (Fig. 6g,h and Supplementary Fig. 37) containing abnormal mitochondria inside the PTECs, distinct from the extrusions and extruded vesicles of normal PTECs containing mitochondria with a healthy morphology (Fig. 4f,i and Supplementary Figs. 20 and 14). These findings again suggest that organelle extrusion belongs to a normal physiological function of healthy PTs.

Conclusion and outlook

This organelle-extrusion-mediated nanoparticle elimination is distinct from conventional membrane-fusion-mediated exocytosis mechanisms. The extruded vesicles (~5 μm) are much larger and contain much

richer intracellular contents, including a variety of organelles, than those vesicles (~100–200 nm or ~1–2 µm) secreted through membrane fusion. This nanoparticle-elimination pathway deepens our fundamental understanding of nanoparticle transport and interactions in the kidneys in addition to glomerular filtration (Extended Data Fig. 1) and ensures the effective elimination of non-biodegradable and even biotransformed nanoparticles after they are actively taken up by the PTs. The observed organelle-extrusion mechanism also sheds light on a long-standing mystery of how mitotically quiescent PTECs remain healthy while carrying out many heavy-duty functions including uptake, metabolism, reabsorption and secretion for the span of an entire life[22]. With this mechanism, PTECs can not only remove unwanted waste from the lysosomes/endosomes but also renew intracellular organelles to maintain homoeostasis without cell division, distinct from other situations when cells have been injured or are under stress[23]. For instance, the extrusion of dysfunctional smooth ER aggregates was observed from proximal tubular cells treated with methyl mercury chloride back in the 1970s (ref. 24). Dysfunctional mitochondria and misfolded proteins can also be released through exophergenesis once the neuronal cells of *Caenorhabditis elegans* are under neurotoxic stress[25]. The ejection of nuclei was observed in the maturation process of red blood cells[26]. Combining our observations with previous findings highlights the diverse self-renewal and self-repair mechanisms that biological systems adapt to maintain homoeostasis under normal and diseased conditions. Continuous investigations on this organelle-extrusion-mediated self-renewal mechanism at the molecular level and potential physiological functions of the extruded vesicles will undoubtedly enrich our fundamental understanding of nephrology and guide us to develop new diagnostics and treatments of kidney diseases, in which nanoparticles can always find incredible roles to play.

Online content

Any methods, additional references, Nature Portfolio reporting summaries, source data, extended data, supplementary information, acknowledgements, peer review information; details of author contributions and competing interests; and statements of data and code availability are available at https://doi.org/10.1038/s41565-023-01366-7.

References

1. Hall, J.E. & Hall, M. E. *Guyton and Hall Textbook of Medical Physiology* (Elsevier Health Sciences, 2010).
2. Du, B. et al. Glomerular barrier behaves as an atomically precise bandpass filter in a sub-nanometre regime. *Nat. Nanotechnol.* **12**, 1096–1102 (2017).
3. Zhuo, J. L. & Li, X. C. Proximal nephron. *Compr. Physiol.* **3**, 1079–1123 (2013).
4. Gudehithlu, K. P., Pegoraro, A. A., Dunea, G., Arruda, J. A. L. & Singh, A. K. Degradation of albumin by the renal proximal tubule cells and the subsequent fate of its fragments. *Kidney Int.* **65**, 2113–2122 (2004).
5. Sancey, L. et al. Long-term *in vivo* clearance of gadolinium-based AGuIX nanoparticles and their biocompatibility after systemic injection. *ACS Nano* **9**, 2477–2488 (2015).
6. Tenten, V. et al. Albumin is recycled from the primary urine by tubular transcytosis. *J. Am. Soc. Nephrol.* **24**, 1966–1980 (2013).
7. Du, B., Yu, M. & Zheng, J. Transport and interactions of nanoparticles in the kidneys. *Nat. Rev. Mater.* **3**, 358–374 (2018).
8. Oh, N. & Park, J.-H. Endocytosis and exocytosis of nanoparticles in mammalian cells. *Int. J. Nanomed.* **9**, 51–63 (2014).
9. Chithrani, B. D. & Chan, W. C. W. Elucidating the mechanism of cellular uptake and removal of protein-coated gold nanoparticles of different sizes and shapes. *Nano Lett.* **7**, 1542–1550 (2007).
10. Balfourier, A. et al. Unexpected intracellular biodegradation and recrystallization of gold nanoparticles. *Proc. Natl Acad. Sci. USA* **117**, 103–113 (2019).
11. Kim, C. et al. Regulating exocytosis of nanoparticles *via* host–guest chemistry. *Org. Biomol. Chem.* **13**, 2474–2479 (2015).
12. Ho, L. W. C., Yin, B., Dai, G. & Choi, C. H. J. Effect of surface modification with hydrocarbyl groups on the exocytosis of nanoparticles. *Biochemistry* **60**, 1019–1030 (2021).
13. Ho, L. W. C. et al. Mammalian cells exocytose alkylated gold nanoparticles *via* extracellular vesicles. *ACS Nano* **16**, 2032–2045 (2022).
14. Tang, S., Huang, Y. & Zheng, J. Salivary excretion of renal-clearable silver nanoparticles. *Angew. Chem. Int. Ed.* **59**, 19894–19898 (2020).
15. Soo Choi, H. et al. Renal clearance of quantum dots. *Nat. Biotechnol.* **25**, 1165–1170 (2007).
16. Christensen, E. I., Rennke, H. G. & Carone, F. A. Renal tubular uptake of protein: effect of molecular charge. *Am. J. Physiol. Ren. Physiol.* **244**, F436–F441 (1983).
17. Xiao, K. et al. The effect of surface charge on *in vivo* biodistribution of PEG-oligocholic acid based micellar nanoparticles. *Biomaterials* **32**, 3435–3446 (2011).
18. Tabata, Y. & Ikada, Y. Effect of the size and surface charge of polymer microspheres on their phagocytosis by macrophage. *Biomaterials* **9**, 356–362 (1988).
19. Jiang, X., Du, B. & Zheng, J. Glutathione-mediated biotransformation in the liver modulates nanoparticle transport. *Nat. Nanotechnol.* **14**, 874–882 (2019).
20. Schuh, C. D. et al. Combined structural and functional imaging of the kidney reveals major axial differences in proximal tubule endocytosis. *J. Am. Soc. Nephrol.* **29**, 2696–2712 (2018).
21. Miller, R. P., Tadagavadi, R. K., Ramesh, G. & Reeves, W. B. Mechanisms of cisplatin nephrotoxicity. *Toxins* **2**, 2490–2518 (2010).
22. Stamellou, E., Leuchtle, K. & Moeller, M. J. Regenerating tubular epithelial cells of the kidney. *Nephrol. Dialysis Transplant.* **36**, 1968–1975 (2020).
23. Fujigaki, Y. Different modes of renal proximal tubule regeneration in health and disease. *World J. Nephrol.* **1**, 92–99 (2012).
24. Fowler, B. A. Ultrastructural evidence for nephropathy induced by long-term exposure to small amounts of methyl mercury. *Science* **175**, 780–781 (1972).
25. Melentijevic, I. et al. *C. elegans* neurons jettison protein aggregates and mitochondria under neurotoxic stress. *Nature* **542**, 367–371 (2017).
26. Moras, M., Lefevre, S. D. & Ostuni, M. A. From erythroblasts to mature red blood cells: organelle clearance in mammals. *Front. Physiol.* **8**, 1076 (2017).

Methods
The full methods are in the Supplementary Information.

Reporting summary
Further information on research design is available in the Nature Portfolio Reporting Summary linked to this article.

Data availability
All data from this work are available in the Article and its Supplementary Information. Source data are provided with this paper. Other relevant data are available from the corresponding authors upon reasonable request for research purposes.

Acknowledgements
We acknowledge the financial support in part from the National Institute of Health (NIH; R01DK124881 (M.Y.), R01DK115986 (J.Z.), R01DK126140 (J.Z.) and R01DK103363 (J.Z.)), National Science Foundation (NSF; 2018188 (J.Z.)), Cancer Prevention Research Institute of Texas (CPRIT; RP200233 (J.Z.)), the University of Texas (UT) at Dallas Office of Research through the Core Facility Voucher Program (award number 11020 to M.Y.) and the Cecil H. and Ida Green Professorship in System Biology (to J.Z.) from the UT Dallas. We also acknowledge the assistance of the UT Southwestern Electron Microscopy Core and the Shared Instrumental Program of NIH (1S10OD021685 (K. Luby-Phelps)). We acknowledge the partial assistance of S. Ahrari at UT Dallas in the synthesis of (−)-AuNPs, and Q. Zhou and S. Li at UT Dallas on some ICP sample preparation. We thank late Dr. Hobson Wildenthal and internal funding support from UT Dallas and K. Luby-Phelps and her staff members at UT Southwestern (UTSW) Medical Center EM core facilities for EM sample preparation; J.-T. Hsieh and his staff members at the UTSW Medical Center for the tissue embedding and providing the HK-2 cell line; G. Meloni and his student R. L. Villones at UT Dallas for providing metallothionein; and Q. Cai at the UTSW Medical Center for her comments on H&E-stained tissue samples.

Author contributions
J.Z., Y.H. and M.Y. conceived the idea and designed the experiments. Y.H. performed most of the experimental studies and data collection. J.Z. recognized the unique organelle-extrusion process during EM imaging of the PTs with Y.H. and M.Y.; J.Z., Y.H. and M.Y. wrote the manuscript. All authors discussed and commented on the manuscript.

Competing interests
The authors declare no competing interests.

Additional information
Extended data is available for this paper at https://doi.org/10.1038/s41565-023-01366-7.

Supplementary information The online version contains supplementary material available at https://doi.org/10.1038/s41565-023-01366-7.

Correspondence and requests for materials should be addressed to Mengxiao Yu or Jie Zheng.

Peer review information *Nature Nanotechnology* thanks the anonymous reviewers for their contribution to the peer review of this work.

https://doi.org/10.1038/s41565-023-01366-7

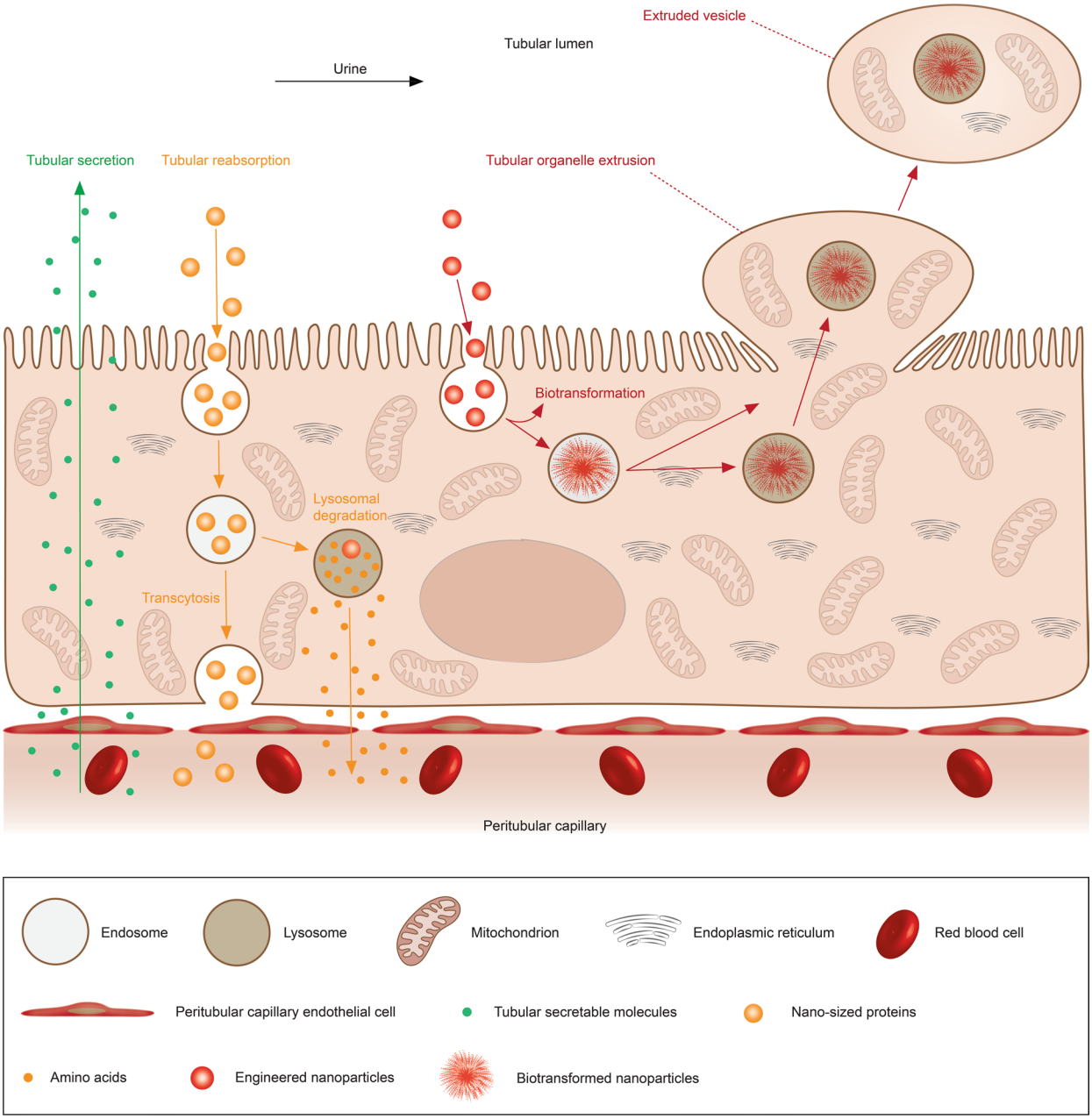

Extended Data Fig. 1 | A schematic summary of substance transport processes carried by proximal tubular epithelial cells (PTECs). PTECs can secrete substances from the blood into the tubular lumen and the urine through transporter-mediated influx- and efflux-processes (green arrow line), reabsorb substances from the lumen back into the bloodstream through transcytosis or transporter-mediated efflux after lysosomal degradation (yellow arrow line). In addition, this newly discovered organelle extrusion of PTECs represents another route to remove the endocytosed and even biotransformed substances back into the tubular lumen for further renal clearance (red arrow line), along with elimination of other intracellular organelles. Since organelle extrusion also happens in healthy proximal tubules without AuNP injection, the physiological function is believed to self-renew intracellular contents and remove wastes to maintain homeostasis without cell division.

nature portfolio

Corresponding author(s): Jie Zheng, Mengxiao Yu

Last updated by author(s): Feb 23, 2023

Reporting Summary

Nature Portfolio wishes to improve the reproducibility of the work that we publish. This form provides structure for consistency and transparency in reporting. For further information on Nature Portfolio policies, see our Editorial Policies and the Editorial Policy Checklist.

Statistics

For all statistical analyses, confirm that the following items are present in the figure legend, table legend, main text, or Methods section.

n/a	Confirmed
☐	☒ The exact sample size (*n*) for each experimental group/condition, given as a discrete number and unit of measurement
☐	☒ A statement on whether measurements were taken from distinct samples or whether the same sample was measured repeatedly
☐	☒ The statistical test(s) used AND whether they are one- or two-sided *Only common tests should be described solely by name; describe more complex techniques in the Methods section.*
☐	☒ A description of all covariates tested
☐	☒ A description of any assumptions or corrections, such as tests of normality and adjustment for multiple comparisons
☐	☒ A full description of the statistical parameters including central tendency (e.g. means) or other basic estimates (e.g. regression coefficient) AND variation (e.g. standard deviation) or associated estimates of uncertainty (e.g. confidence intervals)
☐	☒ For null hypothesis testing, the test statistic (e.g. *F*, *t*, *r*) with confidence intervals, effect sizes, degrees of freedom and *P* value noted *Give P values as exact values whenever suitable.*
☒	☐ For Bayesian analysis, information on the choice of priors and Markov chain Monte Carlo settings
☒	☐ For hierarchical and complex designs, identification of the appropriate level for tests and full reporting of outcomes
☒	☐ Estimates of effect sizes (e.g. Cohen's *d*, Pearson's *r*), indicating how they were calculated

Our web collection on statistics for biologists contains articles on many of the points above.

Software and code

Policy information about availability of computer code

Data collection	Original softwares of instruments used to collect all the data in this work include: Varian UV Cary 50 version 3.00 for absorption spectra collection, Malvern Zetasizer version 7.04 for DLS measurement. Agilent MassHunter Workstation 4.2 for inductive coupled plasma mass spectroscopy measurements, VS-ASW-L100 of Olympus VS120-L100 Slide Scanner for histological imaging and AMT Capture Engine Version 7.00 of JEM-1400+ transmission electron microscope.
Data analysis	OriginLab 2020, NanoMeasure 1.2, cellSense Dimension and ImageJ 1.50 were used for data analysis. Adobe Illustrator CC 2017 was used for drawing figures.

For manuscripts utilizing custom algorithms or software that are central to the research but not yet described in published literature, software must be made available to editors and reviewers. We strongly encourage code deposition in a community repository (e.g. GitHub). See the Nature Portfolio guidelines for submitting code & software for further information.

Data

Policy information about availability of data

All manuscripts must include a data availability statement. This statement should provide the following information, where applicable:

- Accession codes, unique identifiers, or web links for publicly available datasets
- A description of any restrictions on data availability
- For clinical datasets or third party data, please ensure that the statement adheres to our policy

All data from this work are available in the article, its supplementary information, and the source data. Source data is available for Figures 2b, 2c, 2e, 2g, 4b, 5c-5f, 6d and 6f and Supplementary Figures 1a-1e, 3, 9a, 9c, 10b, 10c, 11, 13d, 13e, 19a-19d, 19f, 23i-23k, 30, 32d, 33d, 34b and 34c. Other relevant data are available from the corresponding authors upon reasonable request for research purposes.

Human research participants

Policy information about studies involving human research participants and Sex and Gender in Research.

Reporting on sex and gender	NA
Population characteristics	NA
Recruitment	NA
Ethics oversight	NA

Note that full information on the approval of the study protocol must also be provided in the manuscript.

Field-specific reporting

Please select the one below that is the best fit for your research. If you are not sure, read the appropriate sections before making your selection.

☒ Life sciences ☐ Behavioural & social sciences ☐ Ecological, evolutionary & environmental sciences

For a reference copy of the document with all sections, see nature.com/documents/nr-reporting-summary-flat.pdf

Life sciences study design

All studies must disclose on these points even when the disclosure is negative.

Sample size	No sample size predetermination calculation was performed. Property measurement experiments were repeated at least twice. At least 3 independent samples were included in each experimental group because of the minimum sample size in two-sided Student`s t-test and in one-way ANOVA analysis, which were used in statistical analysis in this work.
Data exclusions	No data was excluded for analysis.
Replication	All key experiments were repeated at least twice with similar results to ensure reproducibility.
Randomization	All mice were randomly allocated for all the animal studies in this work. Cells were also randomly assigned to groups in the cell incubation study.
Blinding	Researchers were not blinded because they were responsible for both doing experiments and analyzing data.

Reporting for specific materials, systems and methods

We require information from authors about some types of materials, experimental systems and methods used in many studies. Here, indicate whether each material, system or method listed is relevant to your study. If you are not sure if a list item applies to your research, read the appropriate section before selecting a response.

Materials & experimental systems

n/a	Involved in the study
☐	☒ Antibodies
☐	☒ Eukaryotic cell lines
☒	☐ Palaeontology and archaeology
☐	☒ Animals and other organisms
☒	☐ Clinical data
☒	☐ Dual use research of concern

Methods

n/a	Involved in the study
☒	☐ ChIP-seq
☒	☐ Flow cytometry
☒	☐ MRI-based neuroimaging

Antibodies

Antibodies used

Antibody was used in the immunohistochemical staining of the kidney tissue sections.
Primary antibody, anti-Metallothionein antibody, product number: ab192385, purchased from Abcam.

Validation

Antibody was verified by the supplier. Validation statements are shown on the manufacturer`s website.
anti-Metallothionein antibody has been validated to be used for immunohistochemical staining and western blot in mouse and human samples. (https://www.abcam.com/metallothionein-antibody-ab192385.html)

Eukaryotic cell lines

Policy information about cell lines and Sex and Gender in Research

Cell line source(s)

HK-2 cell line was purchased from ATCC (CRL-2190).

Authentication

The cell line was not authenticated.

Mycoplasma contamination

The cell line was not tested for mycoplasma contamination.

Commonly misidentified lines
(See ICLAC register)

No commonly misidentified cell lines were used.

Animals and other research organisms

Policy information about studies involving animals; ARRIVE guidelines recommended for reporting animal research, and Sex and Gender in Research

Laboratory animals

BALB/c mice (strain code 047) were purchased from Envigo, both male and female, 6 to 8 weeks, 20 to 25g.
MT-null mice (129S7/SvEvBrd-Mt1tm1Bri Mt2tm1Bri/J, strain code 002211) were purchased from The Jackson Laboratory, both male and female, 6 to 8 weeks, 20 to 25g.
All mice were randomly allocated and housed under standard environmental conditions (23±1 °C, 50±5% humidity and a 12/12 h light/dark cycle) with free access to water and standard laboratory food.

Wild animals

No wild animals were used.

Reporting on sex

Both male and female mice were included for BALB/c mice. Only male mice were included for MT-null mice due to limited number of female MT-null mice.

Field-collected samples

No samples was collected from the field.

Ethics oversight

Animal studies were performed according to the guidelines of the University of Texas System Institutional Animal Care and Use Committee (authorized protocol number: 11-08).

Note that full information on the approval of the study protocol must also be provided in the manuscript.